Heat generation model in the ball milling process of a Tantalum ore

Journal:	*Society for Mining, Metallurgy, and Exploration, Inc.*
Manuscript ID	MMP-16-006.R3
Publication:	Minerals & Metallurgical Processing Journal
Manuscript Type:	Nonmeeting paper
Date Submitted by the Author:	15-May-2016
Complete List of Authors:	Mariño Salguero, Jessica; Universitat Politecnica de Catalunya, Barcelona Industrial Engineering College De Felipe, J.J.; Universitat Politecnica de Catalunya, Escola Politècnica Superior d'Enginyeria de Manresa Jorge, Joan; Universitat Politecnica de Catalunya, Escola Politècnica Superior d'Enginyeria de Manresa Alvarez Rodriguez, Beatriz; Universidad de Leon, Escuela Superior y Técnica de Minas Menendez-Aguado, Juan; University of Oviedo, Mining Engineering
Keywords:	Grinding, heat generation, Ball mills

Heat generation model in the ball milling process of a Tantalum ore

J. Mariño-Salguero[a]., J. Jorge[b], J.M. Menéndez-Aguado[c*], B. Álvarez-Rodriguez[d], J.J. de Felipe[b]
[a] UETIB, Barcelona Industrial Engineering College, Universitat Politècnica de Catalunya (UPC), Spain.
[b] EPSEM, Escola Politècnica Superior d'Enginyeria de Manresa, Universitat Politècnica de Catalunya (UPC), Spain.
[c] Escuela Politécnica de Mieres, Universidad de Oviedo (UNIOVI), Spain.
[d] Escuela Superior y Técnica de Minas de León, Universidad de León (UNILEON), Spain.
*Corresponding autor email: maguado@uniovi.es

Abstract
This work focuses on the characterization of heat generation during dry fracture by direct impact of a Tantalum ore. Moreover, an attempt was made to quantify the heat energy loss to the environment during the grinding process of the ball mill. The study was carried out on mineral samples from a Spanish mine, which was characterized measuring density and specific heat. During the tests, an increase of temperature of 5.9ºC to 7.3ºC after the fracturing process was observed. Then a numerical model was implemented to calculate the temperature distribution through the mill wall. Three possible combinations of heat transfer coefficients (Kapakyulu and Moys; Duda; Heat transfer laboratory UPC) were analyzed. Finally, it was proved that the models with coefficients from Kapakyulu and Moys and Heat transfer laboratory UPC provided the best results in agreement with the experimental data.

Keywords: grinding; heat generation; ball mills.

1. Introduction

Every year, several billion tons of metallic ores, minerals, cement and various other solids used in the ceramic and chemical industries are subjected to size reduction in ball mills throughout the world. U.S. Department of Energy (2005) reported that in the USA about 29% of the total mining industry energy or 0.4% of the total US energy consumption is used in comminution. In Canada and Australia, comminution is responsible for about 2% and 1.5% of total energy use, respectively. In non-industrialized countries where mining constitutes a higher fraction of their industrial sector, comminution costs represent significant contribution to mine operating costs. The specific energy consumption value for grinding of these materials typically ranges from 5 to 50 kWh/ton. Thus, a significant amount of electrical energy is consumed in the ball mill grinding operation (Aguado et al., 2006; Gupta and Sharma, 2014;). Grinding can represent up to 50% of the direct operating cost in a mineral processing plant, especially due to the fact that comminution devices operate in highly inefficient ranges (4-8%) (Wang et al., 2012).

Tavares and King (1998) showed that the cost and energy consumption in fine grinding are considerably larger than those associated with the compressive crushing. This difference in cost and energy consumption has essentially two explanations. As the particle size is reduced, the specific surface area increases. As the particle size approaches to zero, the number of particles and specific surface of all those particles approaches infinity. The amount of energy consumed is a monotonic function of that new surface area. Another explanation is that breakage starts at the micro cracks inside rock particles. As particles get more broken into smaller fragments once and again, these defects are ‘‘consumed” and grindability is reduced in the remaining particles (Tavares and King, 1998). Almost 80% (Aguado et al., 2006) of all the energy supplied to a grinding mill is lost as waste heat, noise, vibration (Cárcamo, 2003) and deformation of rock and equipment (Robert and Schilling, 2000; Schlanz, 1987) instead of creating new surface. Although previous research has been performed on heat generation during fracture, the ways how this energy is lost to the environment or transferred to ball mill parts have not been analyzed in depth. It seems clear that a better understanding of heat transference in milling can be used to improve control and efficiency of milling circuits.

Any small improvement in the efficiency of mill operation could provide an economic benefit to the industries. To achieve this, it is required to understand the dynamic characteristics of grinding (Gupta and Sharma, 2014). There are three different mechanisms of breakage of a particle: Abrasion (shear), cleavage (low speed compression stresses) and fracture (impact – high speed compression stresses). The process of particle size reduction involves all of them, but one might be predominant depending on the type of mill (Monov et al., 2012). The major mechanisms of breakage in ball and rod mills occur mainly by both abrasion and impact

(Sadrai et al., 2011) being the mill geometry of great importance to define in which extent (Dong and Moys, 2001; Dragomir et al., 2014; Whittles et al., 2006).

In the past half century, significant efforts have been dedicated to ball mill modelling and to improve its application in design and optimization (Osorio et al., 2014; Rivera Madrid et al., 2014; Rodríguez et al., 2011).

Three types of models are commonly used: matrix, kinetic and energy models. A general principle in the development of each model is to apply mass balance or energy balance equations. They are related to the mass of the components or the energy involved in the process respectively (Aguado et al., 2006; Monov et al., 2012; Shi and Xie, 2015).

The theory of thermo-elasticity reconciles energy utilized in the deformation of rock, up to the point of crack start. The thermo-elastic stress analysis is based on the principle that the temperature of a solid changes when the stress state does. As long as adiabatic conditions are maintained and the body is loaded within the elastic range, the temperature change is proportional to the change of the sum of the principal stresses. In general, the process of elastic deformation without cracking or damage will consume energy. However the energy for elastic deformation is negligible in comparison to the total energy consumption (less than 1%) (Behera et al., 2007; Cleary and Sawley, 1999; Djordjevic, 2010; Fortsch, 2006; King, 2000; Makokha et al., 2009; Rezaeizadeh et al., 2010; Robert and Schilling, 2000; Rodríguez et al., 2011).

The energy required to particle breaking into of ball mill comes from the rotational energy supplied by the drive motor. The energy is converted to kinetic and potential energy of the grinding media, producing intermittent contacts between particles and boundaries, which can be called as particle sloshing. As result of the particle sloshing, the kinetic energy of the cylinder is rapidly consumed and rolling ceases (Dragomir et al., 2014).

When the mill rotates the grinding charge is raised from a level surface position with liners preventing slippage of the charge so that the media moves with the shell until they fall and tumble down over the mass of the charge. The important characteristics of the charge motion are conventionally termed as cascading, cataracting, and surging. The process of balls rolling down the surface is called cascading (Venugopal and Rajamani, 2001), which results in abrasive type comminution, the impact is negligible, leading to finer grinding and increased liner wear. Whereas those that are thrown out of the surface and follow a parabolic path until the toe of the charge depict cataracting motion, this action leads to impact comminution, which produces coarser products. Cataracting balls hit the mill shell, causing ball-to-wall collision. Finally, the surging impact is when balls collide in midair, which results in ball-to-ball collision (Mishra and Rajamani, 1992). Surging of the charge may take place at all speeds and it is particularly damaging at high speeds (Behera et al., 2007).

To choose the charge volume, it should be taken into account that lower fill levels dissipate energy more efficiently (Hao et al., 2013). But the specific power consumption has a negative impact when the ball mill loading degrees is reduced below a nominal value of 25% of filling (Fortsch, 2006) and the grinding media slides on the liner. Moreover, filling above 45% causes difficulties in the falling process of the balls (Duda, 1977; Ersaym et al.).

The power draw is estimated by the sum of the normal and shear energy, which is lost in all impacts occurring over all slices (Venugopal and Rajamani, 2001). The power draft and grinding efficiency of ball mills depend only of the motion of the grinding charge and the consequent ball collisions that use the input power to cause particle breakage (Mishra, 2003). Even though ball mills have been developed to a high degree of mechanical efficiency and reliability they are still extremely inefficient in terms of energy consumption (Rivera Madrid et al., 2014).

The energy is attempted to be converted into particle breakage through hundreds and thousands of collisions of different intensity and frequency. However, not all impacts may produce particle breakage. As mentioned in (Rajamani, 2000a, Abd El-Rahman et al., 2001), only one thousandth of the impacts in the mill get effective breakage, being the rest of impacts unproductive movements. In general, impacts are of excessive intensity so only a very small part of the energy is utilized in breakage, being the rest lost in frictions or consumed in undesirable slimes generation (Behera et al., 2007). The gross energy input to the mill is consumed in various ways: motion and collisions of balls and material, machine friction, wear of machine parts and balls and so on (Powell et al., 2011). It is accepted that the most reliable models for prediction of drawn power in tumbling mills are based in those developed by Morrell and Austin, and more recently Moys (Austin, et al. 1993; Morrel, 2004; Mulenga and Moys, 2014). Energy losses are accounted through friction in the tangential direction and elastic restitution in the normal direction (Misra and Cheung, 1999).

Mechanical models have been also developed in the last twenty years; discrete element method (DEM) has been used as a practical modeling method of industrial equipment (Agrawala et al., 1997; Farzanegan et al., 2012;). More recently, have been introduced models using SPH (Smoothed Particle Hydrodynamics), CFD (Computational Fluid Dynamics), FEM (Finite Element Method) or their combination (Cleary and Morrison,

2012; Jonsén et al., 2014). The optimization of grinding conditions has normally been determined from the experimental effort and empirical technique (Mori et al., 2014).

There are few thermal models that can be found in the literature (Kapakyulu and Moys, 2007a, 2007b). Van Nierop and Moys (1997) showed that the temperature in a 1.3MW gold mill increases from the feed end to the discharge end. They showed that the difference of temperature along the mill was approximately 5.5 ºC. Van Nierop and Moys (1997) investigated the changes of temperatures in the mill in relation to other variables, mainly mass and power. It was indicated that when the feed of solids to the mill is stopped and the mass decreases, then the temperature increases, tending towards a steady state. The lack of new fresh feed allows the temperature to increase. When the feed is restarted, the mill load mass increases, and the temperature initially decreases, due to the fresh feed, and then decreases to a new steady state (Van Nierop and Moys, 1997).

This work is focused in quantifying the heat losses to the environment during the milling process, in the case of ball mills.

The aims of this work are:

a) Characterizing heat generation during fracture of tantalum ore by thermography images after the breakage by direct impact.
b) To develop a numerical model to predict the heat losses to the environment during the grinding of a ball mill with different conditions of operations (percentage of load and mill speed). The model will be based in the method of control volumes and balance of energy.
c) To prepare and take data of load, indoor air, shell, ambient air temperatures and energy use of a Bond laboratory ball mill, in order to validate the thermal model previously developed, at laboratory scale

2. Methodology

2.1 Heat generation during fracture

In order to increase the knowledge on heat generation when breakage is produced into the ball mill, two experiments were considered: first one was the impact by drop test at different initial height: 30, 40, 50 and 60 cm (2.59–5.19J) considering 73 samples in range from 2.18g to 7.28g of mass; and the second experiment was the impact tests at constant height (60cm-5.19J) applied to 44 samples of different sizes and weight range of 5.26g to 19.3g.

The impact drop weight tests were performed using steel ball of 881 grams which could be positioned at different heights. Once released, the ball falls down freely and hits the ore particle, producing breakage. The thermal behavior in the breakage moment was captured and measured using a thermographic camera.

The Infrared thermal imager used in this work was the FLIR i7 model with a thermal sensitivity of <0,1ºC, accuracy, +/-2% or 2° C, and adjustable operating emissivity from 0.1 to 1.0. The emissivity was 0.94 for all the experiments.

The adjustment was made following the procedure described by the manufacturer. The photos were done at visual angle of 5º to 60º in relation of vertical surface.

The tantalum ore samples used for the tests were bright white of brittle structure and irregular shape with sizes of 15 to 30 mm.

2.1.1 Power draw model

According to Morrell et al. (1991), net power consumption in the grinding process of ball mill is given by following equation:

$$P = \frac{\pi g L N_m r_m}{3(r_m - z r_i)}\left[2r_m^3 - 3zr_m^2 r_i + r_i^3(3z-2)\right] * \left[\rho_c(\sin\theta_s - \sin\theta_T) + \rho_p(\sin\theta_T - \sin\theta_{TO})\right] + L\rho_c\left[\frac{N_m r_m \pi}{(r_m - z r_i)}\right]^3\left[(r_m - z r_i)^4 - r_i^4(z-1)^4\right] \quad (1)$$

$$z = (1 - J_B)^{0.4532} \quad (2)$$

where: r_m internal radius of the mill, J_B fractional ball filling of the mill, L mill length, g gravity constant, r_i the inner surface radius of the charge given by:

$$r_i = r_m\left(1 - \frac{2\pi\beta J_B}{2\pi+\theta_S-\theta_T}\right)^{1/2} \quad (3)$$

β: Fraction of the charge making up the active charge and defined between the toe, the shoulder, the charge inner surface and the mill internal shell.

$$\beta = \frac{t_c}{t_f+t_c} \quad (4)$$

t_c: time for a particle to move from toe to shoulder within the active charge.

$$t_c \approx \frac{2\pi-\theta_T+\theta_S}{2\pi\bar{N}} \quad (5)$$

t_f is the time to move from the shoulder to the toe in free fall during cascading or cataracting.

$$t_f \approx \left[\frac{2\bar{r}(sin\theta_s-sin\theta_T)}{g}\right]^{1/2} \quad (6)$$

$$\bar{N} \approx \frac{N_m}{2} \quad (7)$$

$$\bar{r} \approx \frac{r_m}{2}\left[1+\left(1-\frac{2\pi J_B}{2\pi+\theta_S-\theta_T}\right)^{1/2}\right] \quad (8)$$

ρ_c: average density of the grinding charge in absence of the slurry pool:

$$\rho_c = (1-\varepsilon)\rho_B + \varepsilon US\rho_0 + (1-S)\varepsilon U \quad (9)$$

where ρ_0 is the specific density of the ore.

The angular positions (in radians) of the toe θ_T and shoulder θ_S (see Fig. 1) are given respectively by:

$$\theta_T = 2.5307(1.2796 - J_B)\left[1 - e^{-19.42(\emptyset_C-\emptyset)}\right] + \frac{\pi}{2} \quad (10)$$

$$\theta_S = \frac{\pi}{2} - \left(\theta_T - \frac{\pi}{2}\right)[(0.3386 + 0.1041\emptyset) + (1.54 - 2.5673\emptyset)J_B] \quad (11)$$

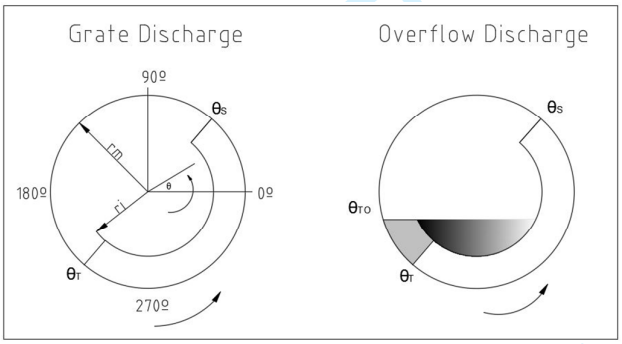

Fig. 1. Simplified shape of the mill charge (Morrell et al., 1992).

Parameter $\emptyset_C$ in Eq. (10), is the experimentally determined fraction of the theoretical critical speed at which centrifugation is fully established. It is given by the following mathematical expressions:

$$\emptyset_C = \emptyset, for\ \emptyset > 0.35(3.364 - J_B) \quad (12)$$

$$\emptyset_C = 0.35(3.364 - J_B), for\ \emptyset < 0.35(3.364 - J_B) \quad (13)$$

2.2 Numerical Thermal model

The overall energy balance for a pilot ball mill in closed circuit is given by:

Total energy supply = Energy lost + Energy accumulate

$$P(t) = Q(t) + S(t) + \frac{dE(t)}{dt} \quad (14)$$

Where P is the net power drawn by the mill and transmitted to the grinding media ($P=P_{\_load}-P_{\_noload}$). P_{noload} accounts the energy lost in the motor, mill bearings and gear box, as well as work done due to friction between

the mill and the surrounding air. This is measured by running the empty mill and measuring the power needed.

S is the rate of energy conversion into sound and vibration. The sound can be considering negligible because is very small (0.004 J/s) compared to the thermal energy loss (Kapakyulu and M. H. Moys, 2007a, 2007b).

dE/dt is the energy accumulated in each element of mill, which is a function of temperature.

$$\frac{dE}{dt} = \sum_{i=1}^{N} \frac{d(m_i C_{pi}(T_i - T_{refi}))}{dt} \tag{15}$$

where T_i, is the temperature of the component under consideration: the temperature of the load (i=1), air above load (i=2), liner (i=3), air gap (i=4) and shell (i=5). T_{refi} is the reference temperature and is taken to be the environmental temperature (T_{env}). Therefore, the term m_i C_{pi} incorporates the mass and specific heat capacity of each element.

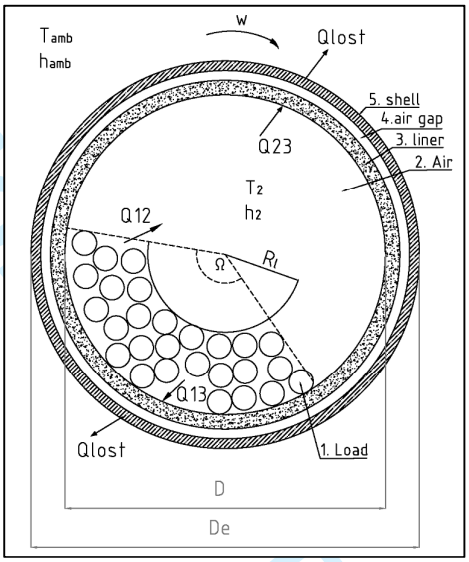

Fig. 2. Heat transfer in transverse section of the ball mill.

Q is the rate of heat transfer from mill to environment. Heat transfer in ball mill is a complex process, including conduction, convection and radiation. The phenomenology of the heat transfer in the cross section of a ball mill is schematically depicted in fig. 2. There are three mechanisms for heat transfer from the boundary of a ball mill from the load: (i) direct heat transfer from the load to wall, (ii) heat transfer from the air to the wall, and (iii) heat transfer between the load and the air.

Besides these three mechanisms, contact heat transfer plays a role among solid particles, while conductive and convective heat transfers contribute to the air heat transfer. It should be noted that the ball mill is operated near room temperature, so that radiative transport may be neglected. The temperature of the load is the result of contact and collision of the grinding media and ore, and friction with the wall of mill also.

2.2.1 Dimensionless formulation

The internal and external convection are governed by Navier-Stokes equations. In the case of forced convection, assuming Newtonian fluid, constant thermophysical properties, transparent medium to radiation and viscosity dissipation negligible, speed is $\vec{v} = (u_r, u_\theta, u_z)$. The equation is written in vector notation as follows:

$$\nabla \vec{v} = 0 \tag{16}$$

$$\frac{\partial \vec{v}}{\partial t} + Re.Pr\vec{v}\nabla\vec{v} = -Re.Pr\nabla p + Pr\nabla^2\vec{v} \tag{17}$$

$$\frac{\partial T}{\partial t} = \nabla^2 T \tag{18}$$

The energy transferred in the cylinder follows the Fourier's theory of conduction heat transfer, to constant physical properties of material, in polar coordinates is given by:

$$\frac{1}{r}\frac{\partial}{\partial r}\left(r\frac{\partial T}{\partial r}\right) + \frac{1}{r^2}\frac{\partial}{\partial \theta}\left(r\frac{\partial T}{\partial \theta}\right) + \frac{\partial}{\partial z}\left(\frac{\partial T}{\partial z}\right) = \frac{\alpha}{\alpha_w}\frac{\partial T}{\partial t} \tag{19}$$

The boundary conditions in the cylinder are:

$$-k_3 \frac{\partial T}{\partial r}\Big|_{r=\frac{D}{2}}^{+} = -k_1 \frac{\partial T}{\partial r}\Big|_{r=\frac{D}{2}}^{-} \qquad \Omega \leq \theta \leq 2\pi \tag{20a}$$

$$-k_3 \frac{\partial T}{\partial r}\Big|_{r=\frac{D}{2}}^{+} = h_{23}(T_2 - T_3) \qquad 0 \leq \theta \leq \Omega \tag{20b}$$

$$-k_3 \frac{\partial T}{\partial r}\Big|_{r=\frac{De}{2}}^{-} = h_{amb}(T_5 - T_{amb}) \tag{21}$$

2.2.2 Problem definition

We consider known all geometric parameters: diameter, D, wall thickness, and length, L; thermophysical properties of materials: thermal conductivity k, density ρ and specific heat cp; environmental conditions (atmospheric pressure Patm and temperature Tenv); operational variables: speed Nm, load percentage J; temperature of load T1.

There are no suitable correlations available in the literature to calculate the convective heat transfer coefficients in the ball mills in function of Reynolds (Re) and Prandtl (Pr) numbers as was determined in the dimensionless analysis. So it have been used three combination of heat transfer coefficient to develop the model:

Case a) the experimental relation founded by Kapakyulu and Moys (2007a, 2007b):

$$hA_{load-wall} = 38.1\emptyset^{0.43}J^{0.2} \tag{22}$$

$$hA_{load-air} = 381\emptyset^{1.72}J^{0.67} \tag{23}$$

$$hA_{air-wall} = 279.7\emptyset^{1.45}J^{0.61} \tag{24}$$

$$h_{env} = 25.2\emptyset^{0.55} \tag{25}$$

Case b) The ball mill operates in a similar way to a rotary kiln. For this reason it has used the experimental expressions of different authors, who studied the heat transfer in rotary kilns (Duda, 1977).

- Load-wall heat transfer coefficient was evaluated using empirical correlation by Tscheng and Watkinsion (1979):

$$h_{13}A_{13} = 11.6k_1\left(\frac{\omega r_{3i}^2 \Omega}{\alpha_1}\right) \tag{26}$$

  In the above expression k_1 is the thermal conductivity of the load, Ω is the angle of fill of the mill, ω is the rotational speed (rad.s-1) and α_1 is the load thermal diffusivity.

- Load-air heat transfer coefficient, according to Ranz and Marshall (1952) under high Reynolds number (Re >100) conditions:

$$Nu = \frac{h_{12}dp}{k_2} = 2 + 1.8Re^{1/2}Pr^{1/3} \tag{27}$$

  where k_2 is the thermal conductivity of the air and dp ball diameter.

- Air-wall considering the correlation of Colburn for a non-established flow in turbulent regime in straight duc:

$$Nu_{23} = \frac{h_{23}D}{k_2} == 0.023Re^{0.8}Pr^{0.3}\left(1 + \left(\frac{D}{L}\right)^{0.7}\right) \tag{28}$$

- The heat transfer coefficient on the outside of the mill shell is governed by forced convection and is independent of the mill filling. For forced convection Re>105.

$$Nu_{env} = \frac{h_{env}De}{k_{env}} = \frac{Re.Pr\sqrt{C_D/2}}{5Pr+5\,ln(3Pr+1)} + \sqrt{2/C_D} - 12 \tag{29}$$

  Where C_D surface drag coefficient (for steel 0.15). This equation was developed by Thermal Transfer Laboratory from UPC (Ivancic et al., 1999).

Case c) It used the Eqs. (22), (34) and (29)

Further, to solve the energy transfer problem some other assumptions have been taking in account to simplify the problem.

- It is a transient problem of heat conduction. The calculation process finishes when the system reaches the steady state. Because the maximum energy loss is in this state, in which all the net power supplied to the mill charge as frictional energy is converted to heat and lost to the environment through the mill shell. The losses by sound and vibration are negligible (Makokha et al., 2009).
- The thermophysical properties of the mill wall are constant.
- The numerical solving considers heat transference in two dimension: radial and circumferential direction, due to the relation L/D of mill is <2.
- The average ambient temperature is constant throughout the study
- The physical changes inside the ball mill do not affect the material volume.
- Overall heat transfer coefficients are constant in the time.
- The temperature of load (T1) is a known constant, which transfers heat to air over the load and to the load–liner interface.
- The convergence criteria is $\varepsilon < 10{-}6$ both for the error of calculation and to reach steady state.
- The wall mill is divided in $n * m$ volumes of different dimensions.

2.2.3 Discretization of equations

It considers a two dimensional situation in polar coordinates, namely r and θ.

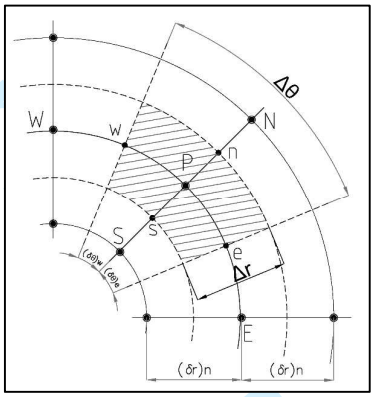

Fig. 3. Control volume in polar coordinates.

After doing the energy balance in each control volume it obtains the discretization equation:

$$a_P {T_P}^{n+1} = a_E {T_E}^{n+1} + a_W {T_W}^{n+1} + a_N {T_N}^{n+1} + a_S {T_S}^{n+1} + b \quad (30)$$

Where:

$$a_E = \frac{k_e \Delta r}{r_e (\delta\theta)_e} \quad a_W = \frac{k_w \Delta r}{r_w (\delta\theta)_w} \quad a_N = \frac{k_n r_n \Delta\theta}{(\delta r)_n} \quad a_S = \frac{k_s r_s \Delta\theta}{(\delta r)_s} \quad a_P^o = \frac{\rho c \Delta V}{\Delta t} \quad b = a_P^o T_P^o \quad (31)$$

(32)

(33)

In the boundary points the discretization equation were modified taking account the energy balances showed in the mathematical formulation Eqs. (20) and (21).

2.2.4 Global algorithm

1. Input data (Geometric and physical properties of materials).

2. Evaluate the power draw model Eq. (27).

3. Assign physical properties to control volumes.

4. Previous calculation mesh and ak coefficients of Eqs. (31) and (32).

5. Stablish initial temperature at time t=0s for all domain; $T_n = T_{env}$;

6. Evaluation of the next time step: $t_{n+1} = t_n + \Delta t$

   6.1 Suppose the next temperature field $T^*_{n+1} = T_n$

   6.2 Form the equation system of all control volumes using the discretization Eq. (30)

6.3 Solve the system with Gauss Seidel method → T_{n+1}

Check convergence of results | $T_{n+1}* - T_{n+1}| < \varepsilon$

No: $T_{n+1}* = T_{n+1}$, and go to 6.2

Yes: go to 6

7. Check steady stead | $T_{n+1} - T_n | < \varepsilon$

No: go to 7

Yes: $T_n = T_{n+1}$ and go to 5

8. Final calculation and print results:

a. Heat loss to environment.

$$Q_{loss} = \sum_{i,j}^{n,m}(Tw_{in\ i,j} - Tw_{out\ i,j}) \quad (34)$$

b. Global heat transfer coefficient.

$$U_{ext} = \frac{Q_{loss}}{Aw_{ext\ i,j}(T_1 - T_{env})} \quad (35)$$

c. Percentage of energy loss in heat form.

$$\% = \frac{Q_{loss}}{P_{net}} \quad (36)$$

9. End.

It validated the numerical thermal model with experimental data of Kapakyulu and Moys (2007a, 2007b), and also the experimental results in this work.

3. Results and discussion

3.1 Physical properties of tantalum ore

The mineral is composed mainly of silicates, with an average rate of 0.01% tantalum. The density measured was 2813 kg/m^3, with relative error of 2.95%. Regarding the specific heat, the experiment yielded the value of 853 J/kg K. The values of density and specific heat obtained are within the magnitude range of standard values of its main components, quartz (>65%) and muscovite (>10%). These variables are used to calculate T1 along with densities and heat capacities of the steel balls used.

3.2 Temperature measurements

The infrared images notice that along the fresh fractures surface there is a temperature increase relative to the not-fractured ore surface. Fig. 4 shows the temperatures reached by two samples after the ore fracture. It was also observed that the increment of temperature was dependent on shape, size and falling height of the test. In the case of more irregular samples, breaking by direct impact was usually partial and temperature of new surface produced was higher than the one obtained with equidimensional particles.

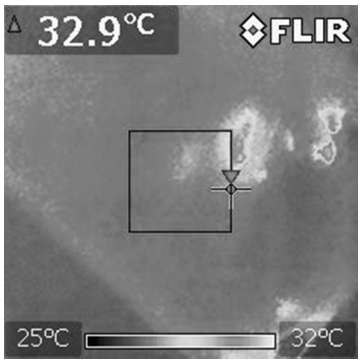

Fig. 4. Infrared images taken after of fracture of sample of 13.53gr-h=60cm

From the first series of test it was observed that increasing intensity of the impact stress produced an increase of temperature along the fractured surface. Specifically, it was observed that at lower potential energy, the increase of temperature along the fracture surface was 5.9ºC while at high energy the increase of temperature along the

fractured surfaces was about 7.3ºC, with also an increase of fracture area.

On the other hand, it was observed that the initial material was not fully fractured. Tromans (2008) theoretically estimated that the mass fractured under indirect tension corresponds to 5–9% for rocks, by conventional comminution. Taking this in account, the quantity of heat generation in the surface fractured was evaluated, (see Figure 5). It was observed that similarly sized particles experience an increased heat generation when the force of impact is greater. The energy not used in breakage is mainly dissipated as heat. The percentage of energy transformed in heat was in range of 30% to 80% of kinetic energy supplied.

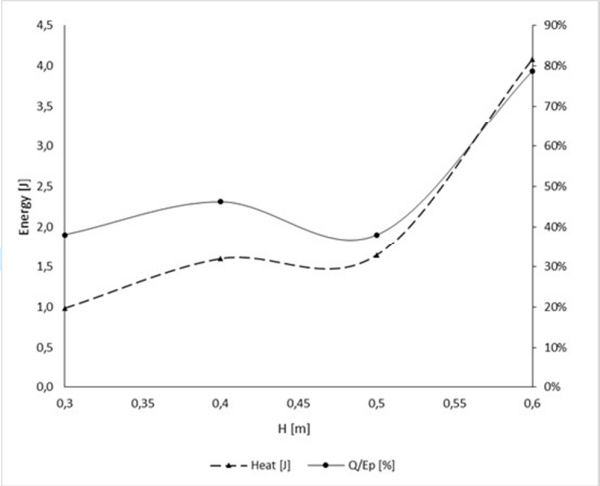

Fig. 5. Heat generation in fracture of samples (2.18g to 7.28g) at different height of impact.

As a result of the second series of tests, it was found that at constant energy supply (60cm-5.19J) the heat generation is also a function of the initial grain size of samples. Smaller particles present higher increase of temperature (8º-10ºC) because the breakage is total and powder product absorbs the excess of energy supplied. Nevertheless, large particles present minor temperature increase because in many case the breakage is partial and the energy is used in produce shear and divide the particle. Fig. 6 shows that temperature decreases exponentially when the mass of particle increases.

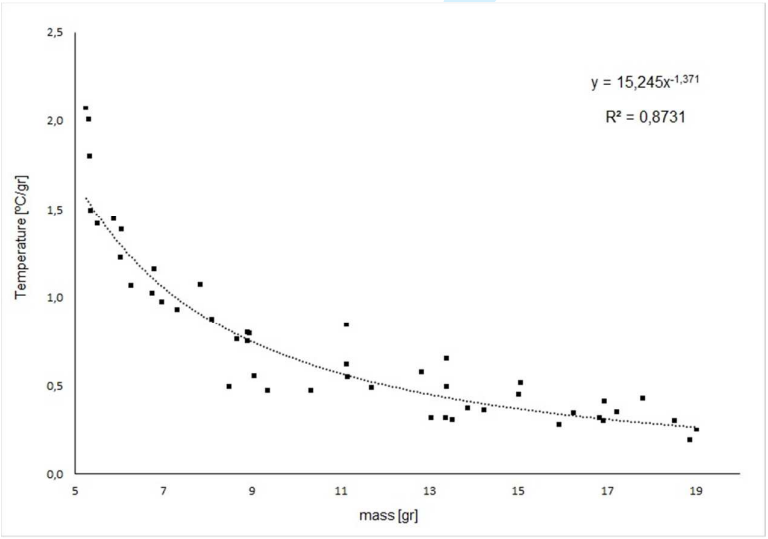

Fig. 6. Specific temperature increase of particles due the impact test, at 60cm of height (5.19J).

These tests helped to determine the degree of magnitude that should supply the load power and energy to the ball mill used.

In order to validate the thermal model developed, a series of tests were performed at laboratory scale. It was selected a standard Bond laboratory ball mill (cylindrical 30 x 30 cm, wall thickness of 19 mm and a total volume of 2580 cm^3). Tests were carried out with different loads and the following parameters were measured: average temperature of the load and balls, indoor air temperature, enclosure temperature, ambient temperature

and power supply.

3.3 Results and validation of thermal numerical model

The numerical model was done using an implicit Euler method to reach the steady state condition. The cylinder grid was divided in 26x18 control volumes. The code was developed in the Matlab R2012b software.

The results of simulation of heat generation in the ball mill studied by Kapakyulu and Moys (2007a, 2007b), are presented in Fig. 7. The temperature distribution around the wall varies in angular and radial direction in the three case of studied. In order to validate of model, the temperature distribution along of the mill's wall was compared among the three cases of study and experimental results. Due to experimental values could only be measured along of an angular position, these were compared with the numerical results of angular position of the highest temperatures, θ=31º clockwise.

For all the combinations of load and mill speed, the proportionality of results between the three models is invariant: with the considerations of heat transfer coefficients b) the temperatures are the highest, and the results obtained with option c) are higher than with case a). But in the case b) the temperature distribution varies only in radial direction. The difference of temperature between the inner and outer side of wall, in the three cases studied, was in the range of 7º-9ºC.

In combinations of lower/middle load and low speed (see Fig.7a, case c) were found closest to the experimental measures. To middle charge and middle speed (see Fig.7b, case b) yielded better results. But for higher speeds Fig. 7c none of three models adjusted to experimental results appropriately. The case a) could be the best option to have a previous view of thermal distribution. Moreover, as the percentage of load and speed increase the case b) and case c) present more similitude in their results.

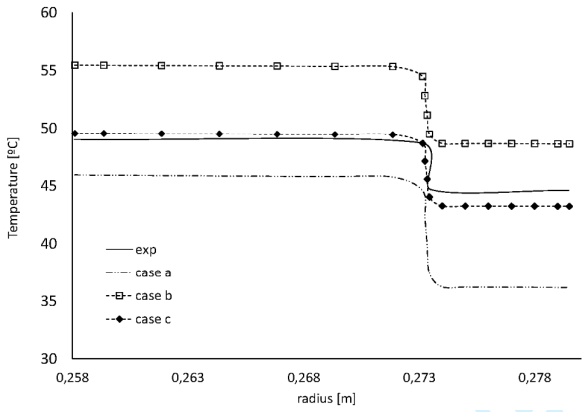

a.

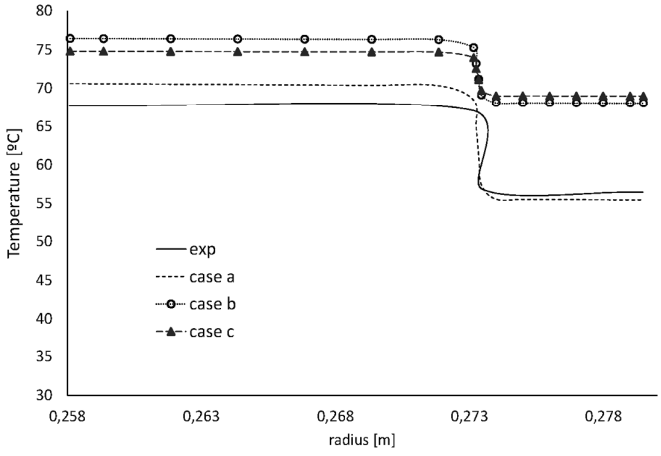

b.

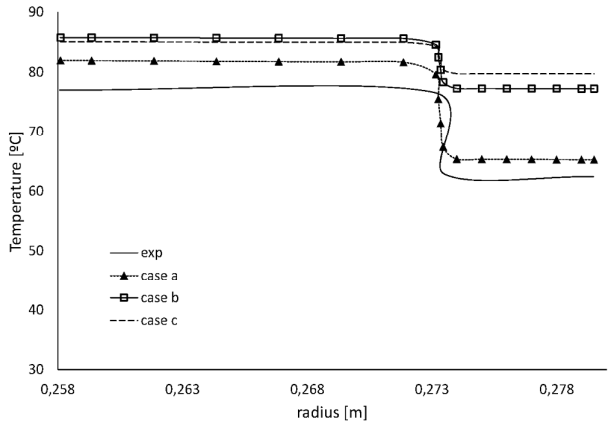

c.

Fig. 7. Temperature distribution along the radial direction at θ=149º in the three cases studied and experimental data for the different combination of charge and critical speed a) 20%-65% 440.5w, b) 30%-75%-760.1w, and c) 40%-85%-923.7w. Pilot ball mill of Kapakyulu and Moys.

The Table 1 is the summary of energy balance for all analyzed combinations. It can be seen that when using the heat transfer coefficients of case a) the quantity of heat loss to the environment is higher than in the other cases. For case a), the range of heat loss is within 45%- 65% of net power supplied. The case b) and case c) show percentages of energy loss about 13% -19%.

The global heat transfer coefficient calculated in case a) is the highest (Ue=8-12W/m^{2}C), whereas in the other two cases the values are around 2-3.8 W/m^{2}C. It must be pointed that although the case c) only differs of the case a) in the heat transfer coefficient for external convection, their results are very different. On the other hand the values of heat transfer coefficients of case b) are higher that case c) but the global coefficient is similar. For these reasons we can conclude that the heat transfer is dominated by external convection.

Table 1 Energy balanced of the pilot ball mill of Kapakyulu and Moys

J [%]-Φ [%] P[w]	***20%-65% 440.5w***			***30%-75% 760.1w***			***40%-85% 923.7w***		
Case	***a***	***b***	***c***	***a***	***b***	***c***	***a***	***b***	***c***
time ss [hours]	2.9	1.8	4.0	3.0	1.8	4.1	3.1	1.8	4.3
h13L [W/m^{2}ºC]	57.5	477.3	57.5	66.8	587.4	66.8	65.0	624.1	65.0
h13A [W/m^{2}ºC]	75.5	347.3	75.5	163.6	545.0	163.6	266.5	767.1	266.5
henv [W/m^{2}ºC]	19.9	3.9	3.9	22.3	4.4	4.4	23.0	4.5	4.5
Qlost [W]	201.8	78.0	59.1	496.0	149.5	139.2	579.3	172.8	162.0
Qrad [W]	1.5	3.4	2.3	3.6	7.1	5.8	4.7	9.5	7.7
Ue [W/m^{2}ºC]	8.0	3.1	2.3	12.2	3.7	3.4	12.8	3.8	3.6
Qlost/Pnet [%]	45.8	17.7	13.4	65.2	19.7	18.3	62.7	18.7	17.5

In the second stage of model validation, it was checked if the model can be used in mills of different sizes. The experimental work was made with 3 different percentages of grinding media and ore J: 11%, 16% and 22%. Finally, the heat loss to environment during grinding in the laboratory ball mill was predicted.

3.4 Discussion of results

According to validation with experimental data from Kapakyulu and Moys (2007a, 2007b), it was found that although the expression for the heat transfer coefficients of the case a) were obtained from measurements made at the pilot ball mill, the results have a relative error in range of 7 to 20% with experimental data. Better accuracy was observed to middle loads with 70-75% of critical speed, and the worst results were in operation condition of low load and low speed.

To overcome the discrepancies of results, the external convection heat transfer coefficient was changed (case c) by an expression based in Re and Pr dimensionless numbers, and independent of J and φ. The accuracy of results for lower loads and speeds improved, being the relative error 2.23%; in the other conditions the results error reached up to 23%.

On the other hand, the case b) had a relative error of approximately 40%, so consequently this combination of heat transfer coefficients is not applicable. Despite the shape of equipment and operation are very similar, the direction of heat transfer was found opposite. However, to analyze the inner heat transfer coefficients, it must be noted that according to the expressions found by Kapakyulu and Moys (2007a, 2007b), 58% of heat from load is

transferred by contact and convection between load and liner, and the rest of energy is transferred to air above the load. In the case b), the proportionality of heat transfer is the same, being the highest value of transference to air.

The value of global heat transfer coefficient is the inverse to the total resist of heat transfer. U totally depend of boundary condition applied in the model, consequently the heat lost calculated by three different model are different.

In the second validation, the ball mill studied had the shell without liner. Only two measures were taken in the wall: the inner and outer temperature, so it was more difficult to verify the accuracy of numerical model. However the cases a) and c) were closer to experimental data, with relative error of 2.4%.

Finally, in the laboratory ball mill, the cases a) and c) results of heat loss through the wall were lower than expected of. For this reason, it would be necessary to perform additional experimental measurements to get a more clear understanding of the problem, because if the distribution of temperature calculated is verified, it means that only one little part of energy is lost through the wall to the environment and then the most of it is kept in the milling products.

4. Conclusions

From experimental observation, it can be concluded that heat generation in the fracture's surface is dominated by the intensity of the impact and also it depends of the sample size. Due to the brittleness of the tantalum ore, samples were comminuted with low level of kinetic energy applied. The particles within the samples with irregular shape and bigger sizes were broken by abrasion, while smaller particles absorbed the total impact which produced fracture in smaller sizes.

The thermography was a practical way to measure the temperature on surface ore after the impact. The changes of temperatures could be observed. Obtained measures were in the range expected in the literature.

A numerical model was developed, which allowed to analyze several combinations of load and mill speed, although results were not as good as expected. Despite that the code converges with low relative error ($1 \cdot 10^{-6}$), the results depended on expressions using convection heat transfer coefficient applied on the boundaries. So, these coefficients do not adequately adjust to this case.

The assumption that temperature distribution is only in two dimensions was confirmed with the experimental work. The ratio between length and diameter was 1.

Both from experimental carried out and Kapakyulu and Moys (2007a, 2007b), data, it can be concluded that the charge temperature initially increases with increasing mill speed. When the mill speed increases, a higher kinetic energy is transferred to the grinding media, which results in more cataracting and therefore higher energy transfer resulting in a higher temperature rise. A higher mill filling leads to a higher power draw, and hence more thermal energy generation.

The heat transfer coefficients charge-liner and charge-air increase as the speed of the mill is increased; and the outside heat transfer coefficient is governed by forced convection due to the speed of the mill, which is independent of the mill filling degree.

Results in the three cases showed bidimensional temperature distributions, but it must be noted that previous works on rotatory kilns showed that at high rotational speed (>3rpm) should not exist fluctuation of temperature in angular direction, and the case could be handled as a one-dimensional problem.

In order to improve the numerical results, it is necessary to find the appropriate expressions of heat transfer coefficient based in Reynolds and Prandtl dimensionless numbers, as were determined in the dimensionless analysis.

This research line is relatively new whereby the development of experimental techniques and testing instruments resistant to hard atmosphere are necessary.

On the other hand, a numerical method to solve the mechanical part as DEM could be combined with the thermal analyses to have a more realistic approximation of heat losses. In this case the initial load temperature was stablished as parameter known, but in a deeper studied, this temperature should be firstly found as a function of shear stress and velocity of slip.

References

Abd El-Rahman, M.K., Mishra, B.K., and Rajamani, R.K., 2001, "Industrial tumbling mill power prediction using the discrete element method," *Minerals Engineering*, Vol. 14, No. 10, pp. 1321-1328.

Agrawala, S., Rajamani, R.K., Songfack, P., and Mishra, B.K., 1997, "Mechanics of media motion in tumbling mills with 3d discrete element method," *Minerals Engineering*, Vol. 10, No. 2, pp. 215-227.

Aguado, J.M.M., Velázquez, A.L.C., Tijonov, O.N., and Díaz, M.A.R., 2006, "Implementation of energy sustainability concepts during the comminution process of the Punta Gorda nickel ore plant (Cuba)," *Powder Technology* , Vol. 170, No. 3, pp. 153-157.

Austin, L.G., Sutherland, D.N., and Gottlieb, P., 1993, "An analysis of SAG mill grinding and liberation tests," *Minerals Engineering*, Vol. 6, No. 5, pp. 491-507.

Behera, B, Mishra, B.K., and Murty, V.V.R., 2007, "Experimental analysis of charge dynamics in tumbling mills by vibration signature technique," *Minerals Engineering*, Vol. 20, No. 1, pp. 84-91.

Cárcamo, H, 2003, "Operaciones mecánicas," Departamento de Ingeniería Metalúrgica, Facultad de Ingeniería y Ciencias Geológicas Universidad Católica del Norte, Antofagasta, Chile.

Cleary, P.W., and Morrison, R.D., 2012, "Prediction of 3D slurry flow within the grinding chamber and discharge from a pilot scale SAG mill," *Minerals Engineering*, Vol. 39, pp. 184-195,

Cleary, P.W., and Sawley, M.L., 1999, "Three-dimensional modelling of industrial granular flows," Second International Conference on CFD in the Minerals Process Industries, December, pp. 95-100.

Djordjevic, N., 2010, "Improvement of energy efficiency of rock comminution through reduction of thermal losses," *Minerals Engineering*, Vol. 23, No. 15, pp. 1237-1244.

Dong, H., and Moys, M.H., 2001, "A technique to measure velocities of a ball moving in a tumbling mill and its applications," *Minerals Engineering*, Vol. 14, No. 8, pp. 841-850.

Dragomir, S.C., Sinnott, M.D., Semercigil, S.E., and Turan, Ö.F., 2014, "A study of energy dissipation and critical speed of granular flow in a rotating cylinder," *Journal of Sound and Vibration*, Vol. 333, No. 25, pp. 6815-6827.

Duda, W., 1977, *Cement data book*. Berlín: Bauverlag GmbH.

Ersaym, S., Sonmez, B., ErgOn, L., Aksanl, B., and Erkal, I.F., "Simulation of grinding circuit at Gümüsköy silver plant, Turkey," Department of Mining Engineering, University of Hacettepe, Ankara, Turkey, pp. C32-C38.

Farzanegan, A., Arabzadeh, B., and Hasanzadeh, V., 2012, "Back-calculation of mechanical parameters of shell and balls materials from DEM simulations," *Journal of Mining and Environment*, Vol. 3, No. 1, pp. 33-40.

Fortsch, D.S, 2006, "Ball charge loading- impact on specific power consumption and capacity," IEEE Cement Industrial Technical Conference.

Gupta, V.K., and Sharma, S., 2014, "Analysis of ball mill grinding operation using mill power specific kinetic parameters," *Advanced Powder Technology*, Vol. 25, No. 2, pp. 625-634.

Hao, L., Lu, Y., Sato, H., Asanuma, H., and Guo, J., 2013, "Analysis on energy transfer during mechanical coating and ball milling-Supported by electric power measurement in planetary ball mill," *International Journal of Mineral Processing*, Vol. 121, pp. 51-58.

Ivancic, A., Oliva, A., Perez Segarra, C.D., and Costa, M., 1999, "Heat transfer simulation in vertical cylindrical enclosures for supercritical Rayleigh number and arbitrary side-wall conductivity", *International Journal of Heat and Mass Transfer*, Vol. 42, pp. 323-343.

Jonsén, P., Pålsson, B.I., Stener, J.F. and Häggblad, H.Å., 2014, "A novel method for modeling of interactions between pulp, charge and mill structure in tumbling mills," *Minerals Engineering,* Vol. 63, pp. 65-72, 2014.

Kapakyulu, E., and Moys, M.H., 2007a, "Modeling of energy loss to the environment from a grinding mill. Part I: Motivation, literature survey and pilot plant measurements," *Minerals Engineering*, Vol. 20, No. 7, pp. 646-652.

Kapakyulu, E., and Moys, M.H., 2007b, "Modeling of energy loss to the environment from a grinding mill. Part II: Modeling the overall heat transfer coefficient," *Minerals Engineering*, Vol. 20, No. 7, pp. 653-661.

Kimura, M., Narumi, M., and Kobayashi, T., 2007, "Design method of ball mill by Discrete element method," *Sumitoko Kagaku*, Vol. II., pp. 1-9.

King, R.P., 2000, "Technical Notes 8 Grinding," Media.

Makokha, B.A., Moys, M.H., Couvas, C., and Muumbo, A.M., 2009, "Steady state inferential modeling of temperature and pressure in an air-swept coal pulverizing ball mill," *Powder Technollogy*, Vol. 192, No. 3, pp. 260-267.

Mishra, B.K., 2003, "A review of computer simulation of tumbling mills by the discrete element method: Part I-contact mechanics," *International Journal of Mineral Processing*, Vol. 71, No. 1-4, pp. 73-93.

Misra, A., and Cheung, J., 1999, "Particle motion and energy distribution in tumbling ball mills," *Powder Technology*, Vol. 105, No. 1-3, pp. 222-227.

Mishra, B.K.K., and Rajamani, R.K., 1992, "The discrete element method for the simulation of ball mills," *Applied Mathematical Modeling*, Vol. 16, No. 11, pp. 598-604.
Monov, V., Sokolov, B., and Stoenchev, S., 2012, "Grinding in ball mills: Modeling and process control," *Cybernetics and Information Technologies*, Vol. 12, No. 2, pp. 51-68.
Mori, H., Mio, H., Kano, J., and Saito, F., 2004, "Ball mill simulation in wet grinding using a tumbling mill and its correlation to grinding rate," *Powder Technology*, Vol. 143-144, pp. 230-239,
Morrell, S., 2004, "A method for predicting the specific energy requirement of comminution circuits and assessing their energy utilisation efficiency", *Minerals Engineering*, Vol. 21, No. 3, pp. 224-233.
Morrell, S., Johnson, G., and Revy, T., 1991, "A comparison through observation and simulation of the power utilization and performance of two dissimilar comminution plants. Fourth Mill Operators," Conference, AusIMM, Australasian Institute of Mining and Metallurgy, Melbourne, Australia, pp. 157–160.
Mulenga, F.K., and Moys, M.H., 2014, "Effects of slurry filling and mill speed on the net power draw of a tumbling ball mill," *Minerals Engineering*, Vol. 56, pp. 45-56.
Osorio, A.M., Menéndez-Aguado, J.M., Bustamante, O., and Restrepo, G.M., 2014, "Fine grinding size distribution analysis using the Swrebec function," *Powder Technology* , Vol. 258, pp. 206-208.
Powell, M.S., Weerasekara, N.S., Cole, S., Laroche, R.D., and Favier, J., 2011, "DEM modelling of liner evolution and its influence on grinding rate in ball mills," *Minerals Engineering*, Vol. 24, No. 3-4, pp. 341-351.
Rajamani, R.K., Songfack, P., and Mishra, B.K., 2000, "Impact energy spectra of tumbling mills," *Powder Technollogy*, Vol. 108, No. 2-3, pp. 116-121.
Rajamani, R.K., Mishra, B.K., Venugopal, R., and Datta, A., 2000, "Discrete element analysis of tumbling mills," *Powder Technology*, Vol. 109, No. 1-3, pp. 105-112.
Ranz, W., and Marshall, W., 1952, "Evaporation from drops," *Chemical Engineering Progress*, Vol. 48, No. 3, pp. 141-146.
Rezaeizadeh, M., Fooladi, M., Powell, M.S., and Weerasekara, N.S., 2010, "An experimental investigation of the effects of operating parameters on the wear of lifters in tumbling mills," *Minerals Engineering*, Vol. 23, No. 7, pp. 558-562.
Rivera Madrid, I.E., Rodríguez, B.A., Bustamante, O., Baena, O.J.R., and Menéndez-Aguado, J.M., 2014, " Ceramic ball wear prediction in tumbling mills as a grinding media selection tool," *Powder Technology* Vol. 268, pp 373-376.
Robert, M.Y, and Schilling, E., 2000, "Attritors and ball mills how they work," Philadelphia Society For Coatings Technology Inc, Akron, Ohio,
Rodríguez, B.A., Menéndez-Aguado, J.M., Coello-Velázquez, A., and Dzioba, B.R., 2011, "Transient state analysis by simulation in a closed grinding circuit," *Minerals Engineering*, Vol. 24, No. 5, pp. 473-475.
Sadrai, S., Meech, J.A., Tromans, D., and Sassani, F., 2011, "Energy efficient comminution under high velocity impact fragmentation," *Minerals Engineering*, Vol. 24, No. 10, pp. 1053-1061.
Schlanz, J.W., 1987, "Grinding: An overview of Operations and Design," North Carolina State University, North Carolina.
Shi, F., and Xie, W., 2015, "A specific energy-based size reduction model for batch grinding ball mill," *Minerals Engineering*, Vol. 70, pp. 130-140.
Tavares, L., and King, R., 1998, "Single-particle fracture under impact loading," *International Journal of Mineral Processing*, Vol. 54, No. 1, pp. 1-28.
Tromans,, D., 2008, "Mineral comminution: Energy efficiency considerations," *Minerals Engineering*, Vol. 21, No. 8, pp. 613-620.
Tscheng, S.H., and Watkinson, A.P., 1979, " Convective heat transfer on rotatory kilns", Canadian Journal of Chemistry, Vol.57, pp. 433-443.
Van Nierop, M.A., and Moys, M.H., 1997, "Measurament of load behaviour in an industrial grinding mil," Control Engineering Practice, Vol. 5, No. 2, pp. 257-262.
Venugopal, R., and Rajamani, R.K., 2001, "3D simulation of charge motion in tumbling mills by the discrete element method," Powder Technology, Vol. 115, No. 2, pp. 157-166.
Wang, M.H., Yang, R.Y., and Yu, A.B., 2012, "DEM investigation of energy distribution and particle breakage in tumbling ball mills," Powder Technology, Vol. 223, pp. 83-91.
Whittles, D.N., Kingman,S., Lowndes, I., and Jackson, K., 2006, "Laboratory and numerical investigation into the characteristics of rock fragmentation," *Minerals Engineering*, Vol. 19, No. 14, pp. 1418-1429.

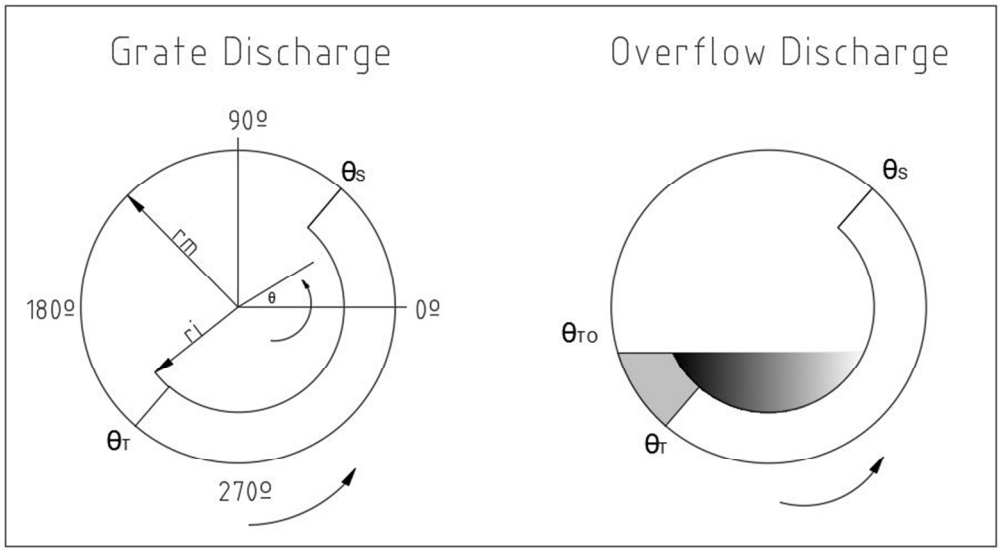

239x131mm (96 x 96 DPI)

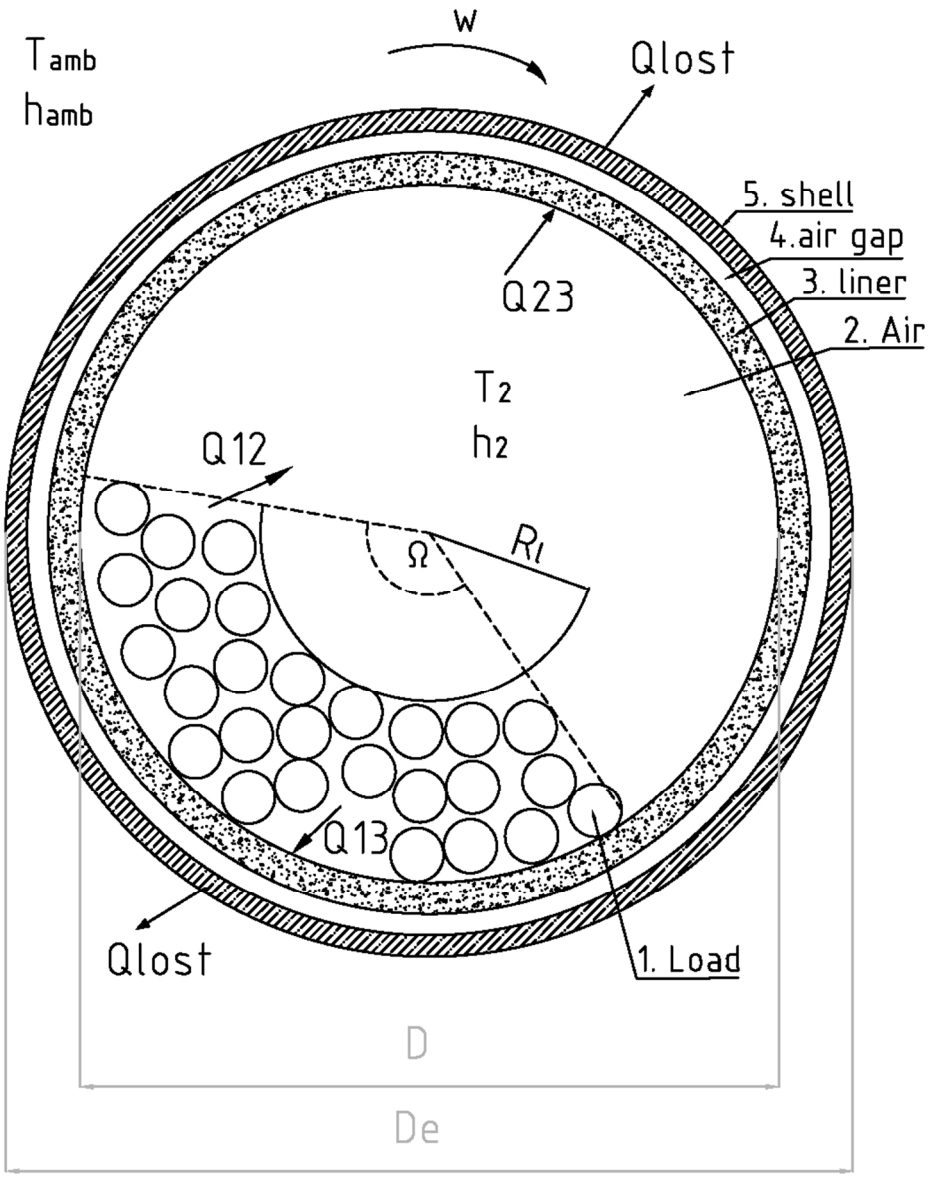

143x172mm (200 x 200 DPI)

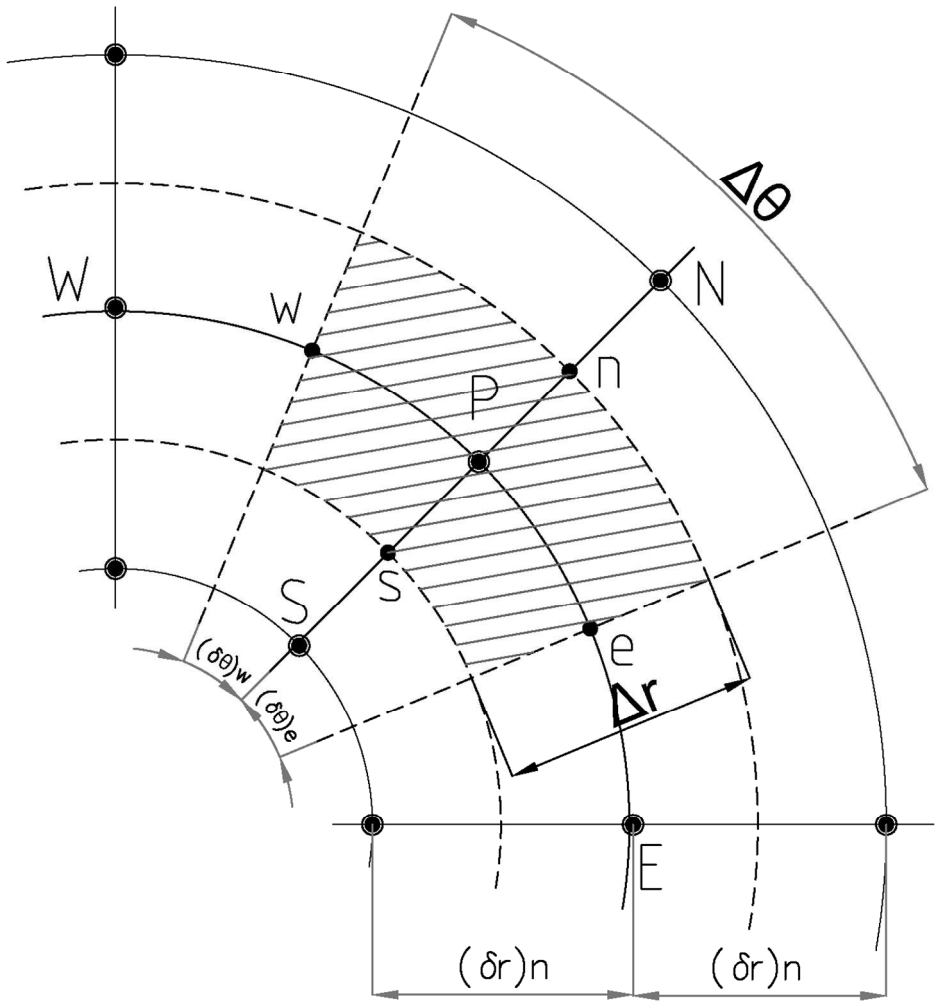

188x199mm (200 x 200 DPI)

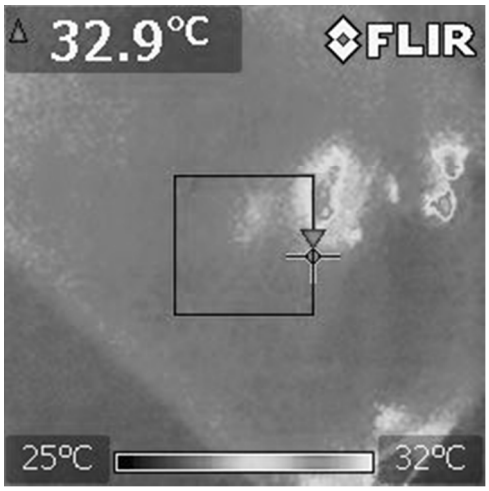

84x84mm (72 x 72 DPI)

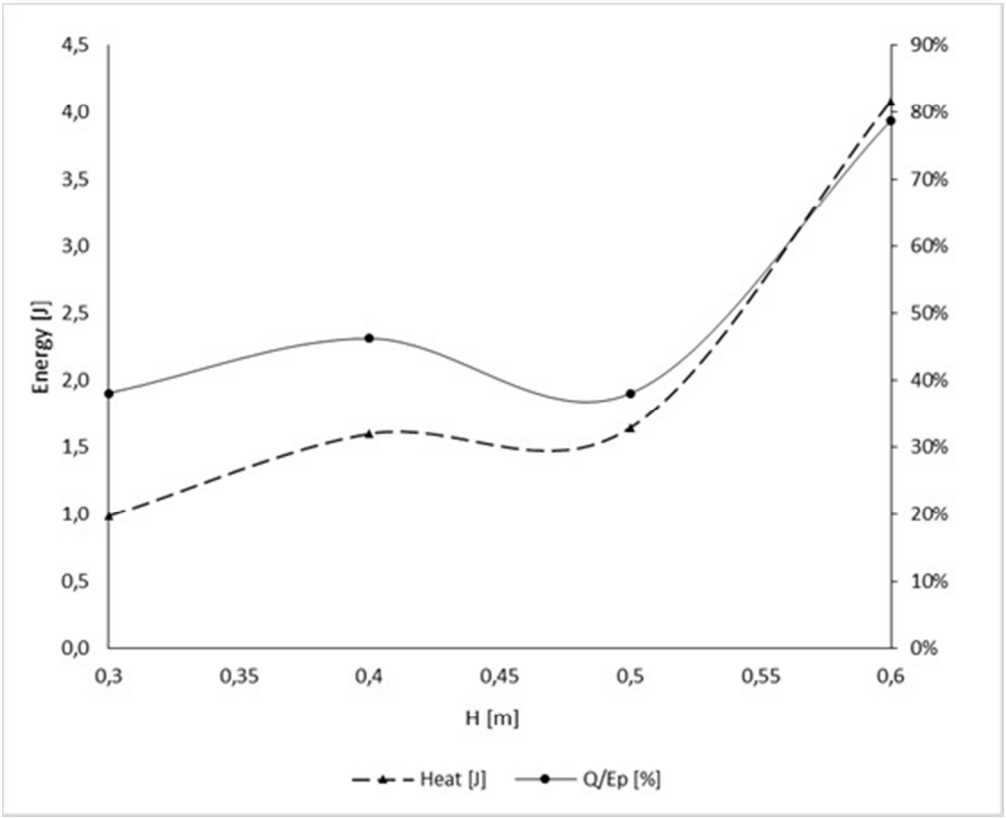

146x119mm (96 x 96 DPI)

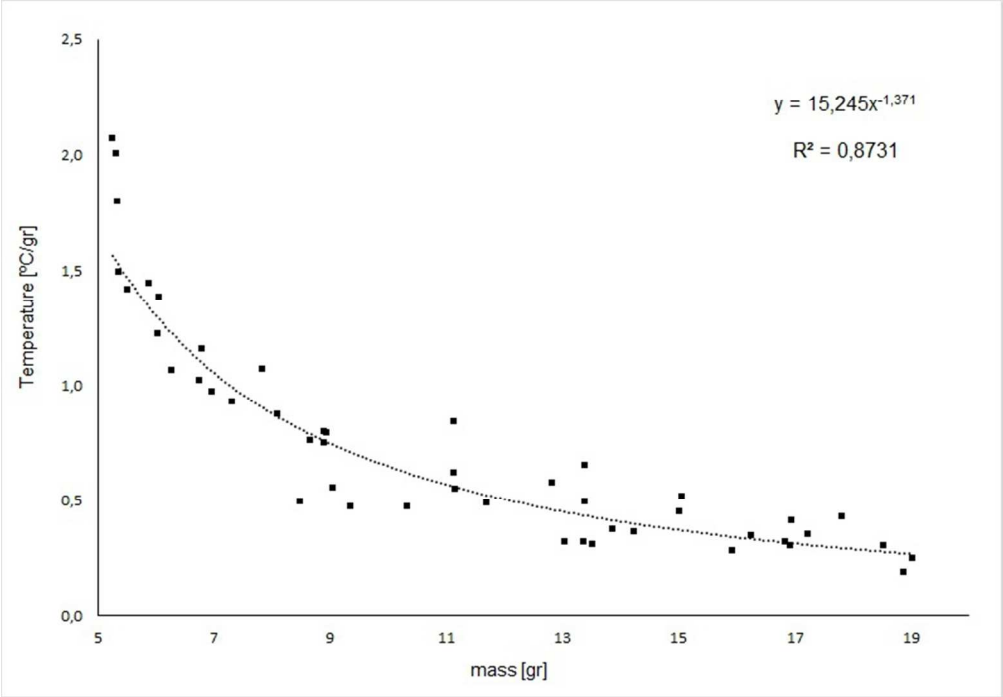

210x146mm (96 x 96 DPI)